Journal of Alloys and Compounds 933 (2023) 167855

Contents lists available at ScienceDirect

Journal of Alloys and Compounds

journal homepage: www.elsevier.com/locate/jalcom

Enhancing hydrogen evolution reaction by synergistically coupling NiMo alloy with Mo on Ni foam

Guanshui Ma [a,1], Yapeng Zheng [b,1], Jiayue Zhang [a], Jiangshan Yan [a], Peng Guo [a], Wei Yang [a], Rende Chen [a], Jianghuai Yuan [a], Li Cui [a], Aiying Wang [a,c,*]

[a] Key Laboratory of Marine Materials and Related Technologies, Zhejiang Key Laboratory of Marine Materials and Protective Technologies, Ningbo Institute of Materials Technology and Engineering, Chinese Academy of Sciences, Ningbo 315201, China
[b] Institute of Materials, Ningbo University of Technology, Ningbo 315016, China
[c] Center of Materials Science and Optoelectronics Engineering, University of Chinese Academy of Sciences, Beijing 100049, China

ARTICLE INFO

Article history:
Received 22 August 2022
Received in revised form 27 October 2022
Accepted 31 October 2022
Available online 2 November 2022

Keywords:
High power impulse magnetron sputtering
Hydrogen evolution reaction
Density functional theory
Synergistic effect
Electrocatalysis

ABSTRACT

The large-scale preparation of non-precious-metal hydrogen evolution reaction (HER) electrodes with remarkable performance was important to the energy crisis. Here, Mo-NiMo/NF (Ni Foam) electrodes were fabricated by homemade high power impulse magnetron sputtering technique with subsequent annealing. The synthesized Mo-NiMo/NF electrodes presented an exceptional electrocatalytic performance with $\eta 10$ = 71 mV and prominent stability in alkaline aqueous electrolyte for the HER. The experimental data were corroborated by density functional theory (DFT) calculations. The significant catalytic performance for HER active arose from NiMo alloy and the coupling effect between Mo and NiMo alloy. The lowest value on Gibbs free energy of NiMo was − 0.027 eV, very close to the ideal value zero. The adsorption energy of hydrogen atom from heterojunction between Mo and NiMo was − 1.786 eV, which could facilitate Volmer step to further enhance HER activity. More importantly, this synthesis method reported here was scalable, which could provide a valuable strategy to engineer the electrocatalysts with the aim to improve their catalytic activities.

1. Introduction

Hydrogen energy, as the cleanest second energy source, has become an important energy strategy to relax the energy crisis around the world. Specifically, hydrogen owns the highest gravimetric energy density between 120 and 142 MJ/kg, which is about three times higher than gasoline and 150 times higher than a lithium-ion battery. When hydrogen is burned with oxygen, in addition, the only combustion product is clean water and heat [1–4]. Among the approaches developed thus far for hydrogen production, water electrolysis has demonstrated its inherent superiority in the views of its low cost and environmental benignity [5,6]. During the process of water electrolysis, electrocatalysts play a pivotal role in the energy conversion efficiency for hydrogen evolution reaction (HER) [7–9]. Nowadays, precious metal based electrocatalysts such as Pt/Pd-based catalysts are widely developed towards HER. However, the high cost and scarcity of these materials largely hamper their widespread applications. The inexpensive electrocatalysts with excellent efficiency and stability are thereby of great importance as the alternative HER candidates [10–14].

Among the developed non-precious metal-based catalysts, nickel is well-known for hydrogen production due to its low price and the higher exchange current density in HER. However, under aggressive alkaline conditions, nickel displays poor corrosion resistance because it is easy to agglomerate during the process of catalytic cycling. Therefore, various nickel-based compounds including oxides [15,16], sulfides [17], phosphide [18,19] and nitrides [20–24] have been widely studied as electrocatalysts for HER. In particular, the NiMo alloy for HER draws much attention due to the achieved good wear resistance, high corrosion resistance as well as superior electrocatalytic properties [25–32]. For example, Wang et al. [33] prepared a three dimensional porous Ni-Mo film with thickness of 180–240 mm, where the outstanding catalytic performance with an

* Corresponding author at: Key Laboratory of Marine Materials and Related Technologies, Zhejiang Key Laboratory of Marine Materials and Protective Technologies, Ningbo Institute of Materials Technology and Engineering, Chinese Academy of Sciences, Ningbo 315201, China.
E-mail address: aywang@nimte.ac.cn (A. Wang).
[1] Authors contributed equally to this work.

https://doi.org/10.1016/j.jallcom.2022.167855
0925-8388/

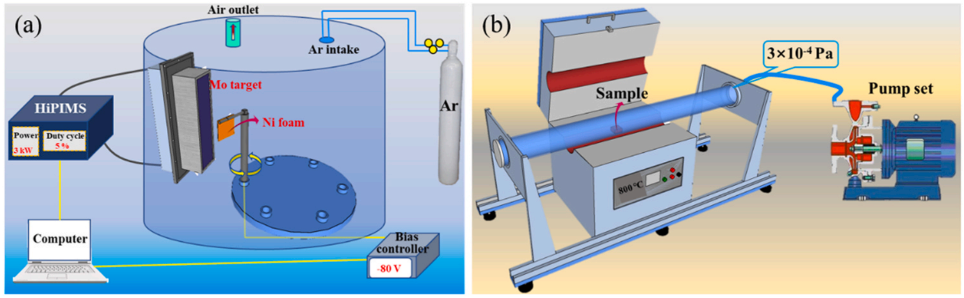

Fig. 1. (a) Schematic of HiPIMS process for Mo/NF preparation, (b) Schematic model of Mo/NF annealing treatment to generate Mo-NiMo/NF.

overpotential of 47 mV at 100 mA cm^{-2} for HER was reported. Du and co-worker [34] presented that Mo in Ni_4Mo was oxidized and dissolved in form of MoO_4^{2-}, which could both enhance the durability of Ni_4Mo alloy and stimulate the HER activity of Ni. Mert et al. [35] found that the Mo content significantly affected the electrocatalytic activity and stability of Ni–Mo coating for HER, the higher Mo content of the coating was, the highest electrocatalytic activity was yielded. In this case, the above-mentioned results provide a new strategy to improve the performance of nickel based HER catalysts by synergistically integrating Mo and NiMo.

Recently, numerous methods have been used to fabricate Ni-Mo alloys toward HER catalysts, such as mechanical alloying [36,37], electrolytic deposition [38], plasma spraying and arc ion plating [39], high energy ball milling [40], gel-combustion [41,42] and physical vapor deposition (PVD) [43]. Comparing with the other technologies, PVD gives the priority on facile deposition over large uniformity and low temperature for mass production with wide usage of substrates [44,45]. Specifically, high power impulse magnetron sputtering (HiPIMS) [46], as a new PVD technology firstly introduced in 1997, favors a high plasma density together with a high metallic ionization rate than most of traditional direct current (DC) or radio-frequency (RF) magnetron sputtering. Increased metallic ionization rate can significantly inhibit unnecessary target poisoning during reactive sputtering [47]. It can also improve the bonding strength between coating and substrate and the corrosion resistance of the coating by adjusting the structure of the metal elements.

In this work, we fabricate the Mo-NiMo coatings on nickel foam (Mo-NiMo/NF) as cost-effective cathode for HER by a comprehensive technique composed of a homemade HiPIMS deposition system with subsequent vacuum annealing. The Mo-NiMo/NF electrode presents electrocatalytic activity with the overpotential as low as 71 mV at 10 mA cm^{-2} and the Tafel slope of 104 mV dec^{-1}. In addition, the prepared Mo-NiMo/NF can be well maintained with only slight 1.0% decrease within 24 h, displaying a good long-term durability for HER. Furthermore, density functional theory (DFT) calculations are executed to clarify the mechanism of obtained Mo-NiMo/NF with outstanding HER activities. Due to the synergistic effect of alloying NiMo and heterojunction (between NiMo and Mo) in electronics, the Mo-NiMo/NF electrode can be used as an efficient electrocatalyst for HER.

2. Experimental

2.1. Preparation of Mo-NiMo/NF cathodes

The NF was ultrasonically pretreated in 1 M hydrochloric acid for 2 min to remove the oxide layer on the surface. Subsequently, the NF was rinsed with water and acetone in sequence and dried with high-purity nitrogen gas. The Mo-NiMo coating was deposited on NF substrate by a home-made HiPIMS deposition equipment along with the extra vacuum thermal annealing. The substrate holder was rotated continuously at a speed of 5 rpm throughout the deposition process to ensure a uniform distribution of thickness and elements on the substrate. Fig. 1**a** and **b** showed the system schematics for HiPIMS and thermal annealing, respectively. The Mo target with purity of 99.99% was used as the sputtering source. In order to eliminate residual atmosphere in chamber, the base vacuum was pumped down a 3×10^{-5} Torr before deposition. Furthermore, the target surface was etched by Ar ions for 10 min to eliminate the contaminations. During etching and deposition, a pulsed DC bias of − 80 V was always applied to the substrate. The HiPIMS mode with applied power of 3.0 kW and duty cycle at 5% for 10 h was used to fabricate Mo coating on NF substrate. Finally, the Mo/NF sample was treated at 800 °C for 1 h with 3.0×10^{-4} Pa vacuum to achieve the Mo-NiMo/NF cathode.

2.2. Materials characterization and electrochemical measurements

The surface microstructure and element composition of as-prepared samples were performed on scanning electron microscope (SEM) with an energy dispersive X-ray (EDX) analyzer at 15 kV. The high-resolution transmission electron microscopy (HRTEM) analysis was carried out on Talos F200. The phase structure of samples was recorded by power X-ray diffraction (XRD). The bonds state and chemical composition were performed by X-ray photoelectron spectroscopy (XPS).

Electrochemical properties of samples were carried out by the Gamry electrochemical workstation in a standard three-electrode cell at room temperature, during which the work area was normalized to 1 cm^2. The line scan voltammetry (LSV), chronoamperometry (CA) and electrochemical impedance spectroscopy (EIS) analysis could be performed successively. The electrolyte was 1 M KOH purged with N_2 gas (99.998%) for 1 h. An Ag/AgCl electrode was regarded as the reference electrode, a graphite stick was used as the counter electrode, the fabricated Mo/NF, Mo-NiMo/NF and NF were used as the working electrodes, respectively. All polarization curves without iR-corrected in the experiment, and all the potentials in electrochemical measurements were calibrated by the following equation:

$$E(RHE) = E(Ag/AgCl) + 0.194 + 0.05916 \times pH \quad (S1)$$

2.3. Theoretical calculations

The first-principles calculation of HER was performed via Vienna ab-initio simulation package (VASP) code [48,49]. The projector-augmented wave (PAW) method represented the core-valence interaction of elements [50]. The valence electron configurations for Ni, Mo and H were $3d^84s^2$, $4p^64d^55s^1$ and $1s^1$, respectively. The exchange-correlation function was represented by generalized gradient approximation in the form of Perdew-Burke-Ernzerhof [51]. The dipole correction along z axis was implemented to remove additional interaction caused by asymmetric surface of slab models. The cutoff energy of the plane-wave basis was set as 400 eV. The

Brillouin zone was sampled with gamma-centered k-mesh densities of $2\pi \times 0.05$ Å^{-1}. The long-range van der Waals interactions were treated by the zero damping DFT-D3 method of Grimme [52,53]. The convergency criteria of energy was set as 1×10^{-4} eV/atom and the force on each atom was set as 0.05 eV/Å. DFT+U method was adopted to correct the self-interaction error and Hubbard-type correction with effective 6.3 eV was respectively applied on the 3d and 4d orbitals of Ni and Mo [54,55].

The Gibbs free energy (ΔG_{H^*}) could be calculated by:

$$\Delta G_{H^*} = \Delta E_{H^*} + \Delta E_{ZPE} - T\Delta S \quad (S2)$$

where ΔE_{H^*}, ΔE_{ZPE} and ΔS were the adsorption energy of hydrogen atom, zero point energy correction and entropy change, respectively. Because the entropy of hydrogen in absorbed state was disregarded, ΔS was thus simplified as $-1/2\ S_0$ (S_0 was the entropy of H_2 in the gas phase at standard conditions, 1 bar of H_2 and pH = 0 at 300 K). As a result, the free energy of the adsorbed state might be presented as:

$$\Delta G_{H^*} = \Delta E_{H^*} + 0.24 \quad eV \quad (S3)$$

The ΔE_{H^*} was calculated by:

$$\Delta E_{H^*} = E_{sur-H} - E_{sur} - 1/2E_{H2} \quad (S4)$$

where $E_{sur\text{-}H}$ was the energy of slab with adsorbed hydrogen atom, E_{sur} and E_{H2} were the energy of clean slab and the energy of molecular H_2 in the gas phase, respectively [23].

3. Results and discussion

Fig. 2 showed the fabrication process of the Mo-NiMo/NF. Firstly, the pretreated NF substrate was loaded into the homemade HiPIMS deposition system. Then the Mo coating was deposited by sputtering on NF, corresponding the turned gray color observed for Mo/NF sample (Fig. S1, supplementary information). Subsequently, the acquired Mo/NF sample was annealed in vacuum at 800 °C for 1 h, which made the color change to atropurpureus for Mo-NiMo/NF sample (Fig. S1, supplementary information).

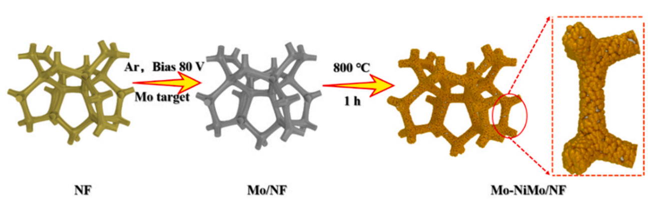

Fig. 2. A schematic of the preparation process for the Mo-NiMo/NF.

The low magnification SEM images of untreated NF showed a three-dimensional (3D) structure at submicron scale, and it was observed that the surface of bare NF skeleton was smooth with quantities of grain boundaries at high magnification (Fig. S2, supplementary information). Fig. 3 showed the SEM images and EDX of Mo/NF. It exhibited that the foam still maintained a 3D skeleton structure after the deposition. At high magnification, it was observed that the surface of the cathode became rougher than that of NF, and the grain boundaries were fully covered by Mo. The EDX spectrum further revealed that the modified Mo was successfully deposited onto the NF (Fig. 3e). Moreover, the atomic fraction of Mo:Ni was approximately 93:7, revealing that a great quantity of Mo was deposited on NF, which was to facilitate the preparation of heterojunction structures. Moreover, the elemental mappings for Mo/NF showed that the Mo element distributed homogeneously on NF.

Fig. 4a showed the cross-sectional micrograph of the as-deposited Mo coating. It was obvious that the Mo coating displayed columnar crystal structure with a thickness around 3.20 µm. The EDS line scanning profile was adopted to further investigate the structure of the cross-sectional and the formation of interface. As shown in Fig. 4b, Mo was not disappeared completely and the Ni was not increased sharply at the interface. The phenomenon may be attributed to that the power of HiPIMS is relatively high, resulting of high energy of the Mo atoms. The Mo atoms are pushed into the surface of the NF, and some nickel atoms are knocked out, forming a back sputtering. Fig. 4c and 4d showed the cross-sectional micrograph and corresponding EDX line of the Mo-NiMo coating. It was apparent that the coating displayed good uniformity and dense structure with a thickness about 3.22 µm after annealing. It was clear that from the coating to the substrate Mo element decreased gradually while Ni element increased gradually. The phenomenon was due to the elemental interdiffusion between substrate and coatings during heat treatment. The adherent interface between coating and substrate was clear and relatively sharp, without any defects, such as

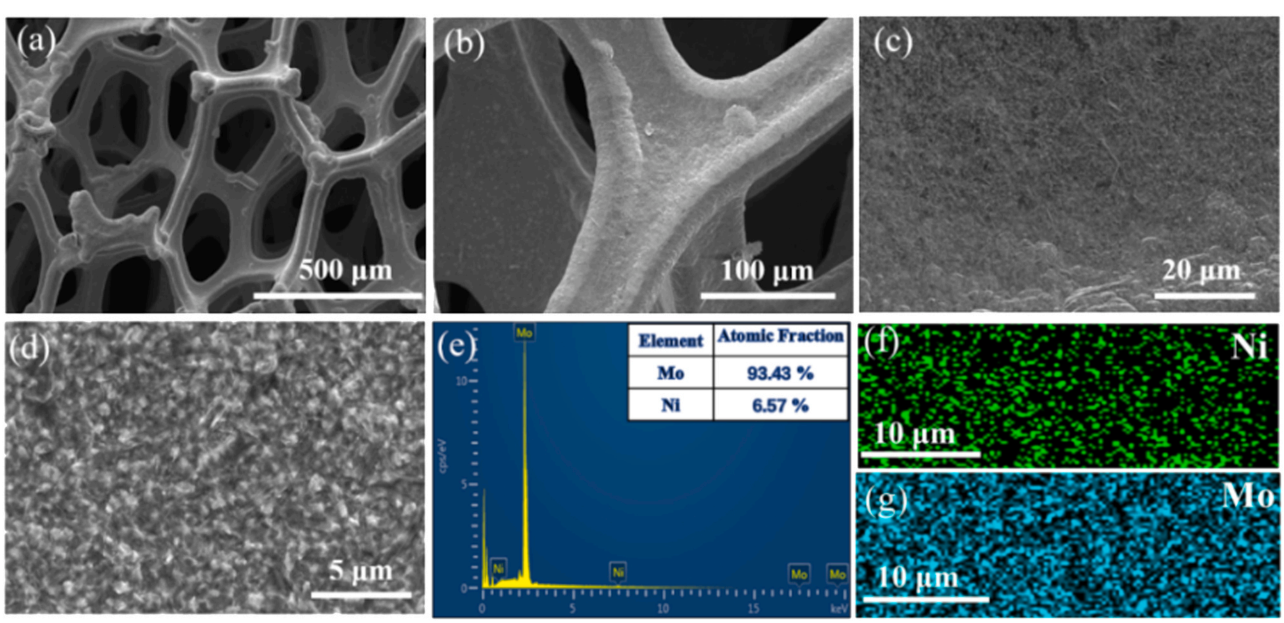

Fig. 3. SEM characterization of Mo/NF. (a) and (b) low magnification, (c) and (d) high magnification, (e) EDX pattern, the inset is the element atomic fraction, (f) and (g) EDX element mapping.

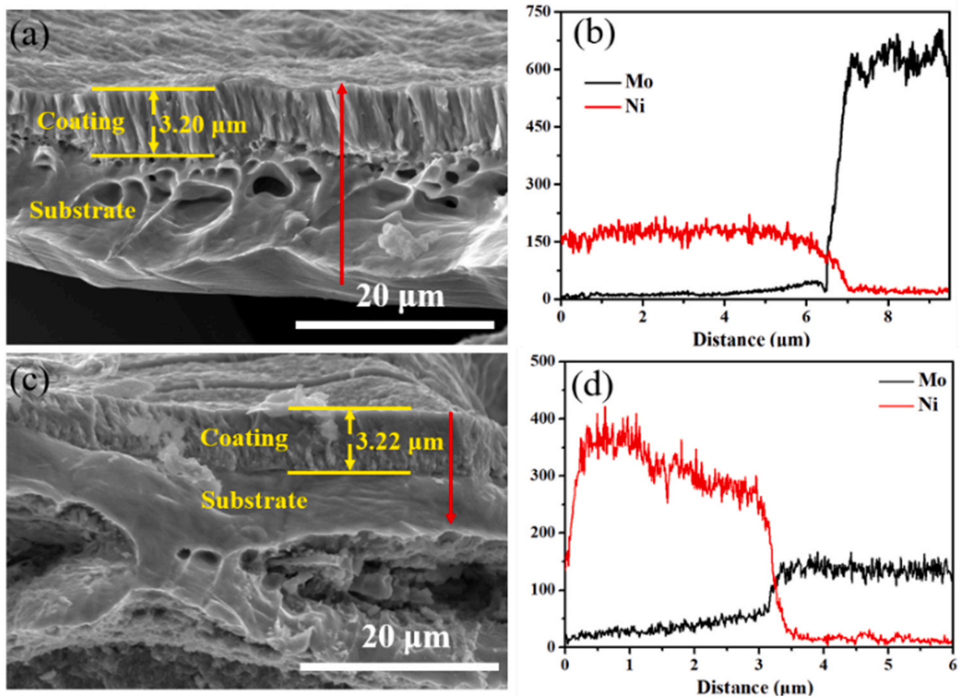

Fig. 4. (a) Cross-sectional morphologies of the Mo/NF sample. (b) EDX scanning red line in (a), (c) Cross-sectional morphologies of the Mo-NiMo/NF sample. (d) EDX scanning red line in (c).

columnar and cracks. Combined with the EDX mapping result (Fig. S3, supplementary information), we suggest the nickel element reaches the surface of the coating through thermal diffusion.

The crystalline phases of the prepared electrodes characterized by XRD were shown in Fig. 5a. For the bare NF, the observed 2θ around 44.6°, 51.8°, 76.4° and 92.9° were corresponding to the diffraction peaks (111), (200), (220) and (311) of Ni (JCPDS #04–0850). After the deposition of Mo on NF, the diffraction peaks (JCPDS #42–1120) of Mo could be found around 40.6°, 73.7° and 87.9°, which were corresponding to the crystal faces (110), (211), (220). The appearance of those peaks meant that the Mo had been successfully deposited on the NF skeleton surface, which was consistent with SEM images in Fig. 3**.** Moreover, the observed 2θ around 37.6°, 39.4°, 59.9° and 73.3° belonged to the diffraction peaks (123), (040), (351) and (071) of NiMo (JCPDS #48–1745). The results displayed that NF and Mo had formed the NiMo alloy during annealing process.

XPS technique was further adopted to characterize the change of surface electric states and chemical composition of the prepared electrodes. Fig. 5b showed three peaks of Mo 3d XPS spectrum, among which the peak located at 228.0 eV belonged to the Mo^0 2d$_{5/2}$, while the peaks at 232.2 eV and 235.6 eV represented Mo^{6+} 3d$_{5/2}$ and 3d$_{3/2}$, respectively [25,30]. The high-valence state of Mo might be ascribed to a small amount of Mo oxide, which was derived from surface oxidation with the exposed air [56]. The deconvoluted high-resolution Ni 2p XPS spectrum by peak fitting in Fig. 5c illustrated five peaks. The peaks located at 856.2 eV, 858.7 eV and 873.8 eV were attributed to Ni^{2+} 2p$_{3/2}$ and 2p$_{1/2}$, while the peaks resided at 861.7 eV and 879.9 eV belonged to their satellite peaks, matching well with NiMo alloy [57,58]. Combined with the analyses of the XRD, it indicated that Mo and NiMo alloy were successfully fabricated on NF.

In order to demonstrate the performance of the cathodes, the electrochemical activities of the as-prepared Mo-NiMo/NF electrode towards HER were evaluated by LSV measurements at a typical three-electrode system (Fig. 6a). Because of the dissolved Pt would positively contribute to activity during HER, a graphite stick instead

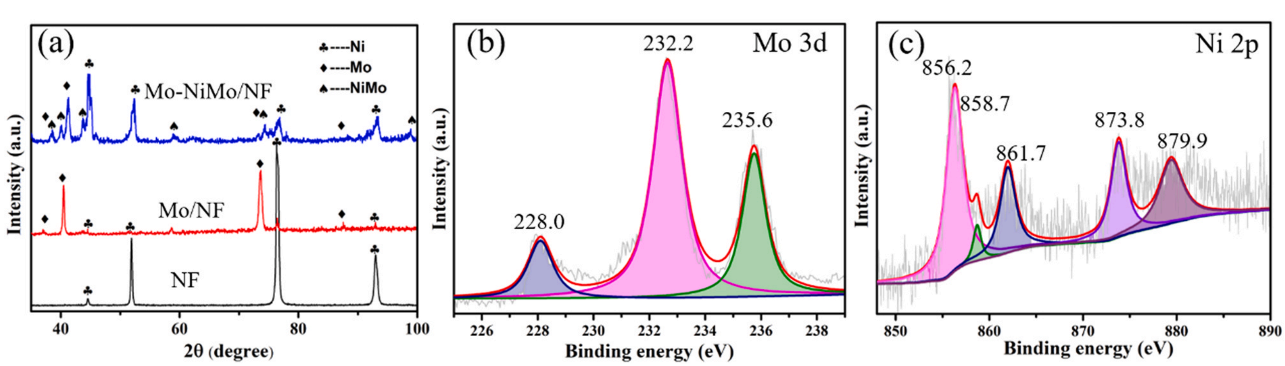

Fig. 5. (a) XRD spectrum of NF and treated NF, (b) Mo 3d and (c) Ni 2p core level XPS spectrum of the Mo-NiMo/NF.

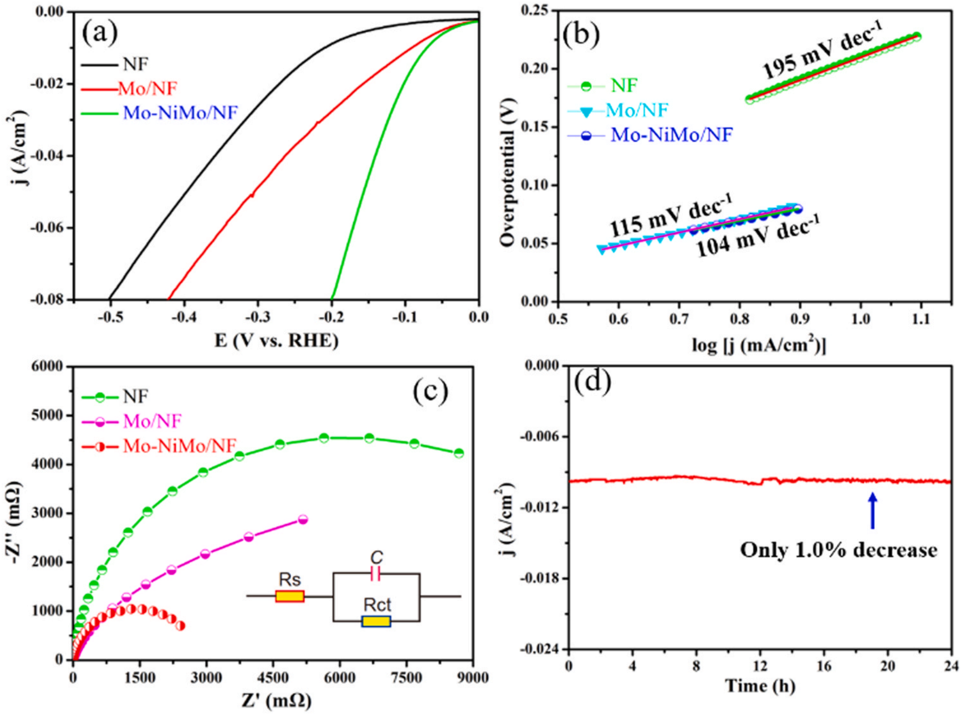

Fig. 6. HER performance of the treated NF and pristine NF (a) Linear sweep voltammetry, (b) Tafel plots, (c) Nyquist plots at an overpotential of 200 mV in 1 mol L^{-1} KOH with the frequency range of 10^5-0.01 Hz, the inset shows the fitted equivalent circuit. (d) Chronoamperometry curve of Mo-NiMo/NF at a constant overpotential of 71 mV.

of a Pt wire/coil was used as the counter electrode. For comparison, the HER activities of the Mo/NF and pristine NF electrodes were also examined under the same conditions. The LSV curves were shown in Fig. 6a. The overpotential at 10 mA cm^{-2} (defined as η10) was usually used to compare the activities of various catalysts, and a smaller η10 indicated a higher activity. It was clearly seen that the Mo-NiMo/NF showed the lowest overpotential of η10 = 71 mV among the prepared cathodes, which was much smaller than those of the pristine NF and Mo/NF (the particular data in Table 1). And this was a marked low value compared with many other Ni-based catalysts as informed in previous work [22,59]. It was knowledge that further increase of cathodic potential might lead to a sharp rise in the cathodic current. The overpotentials of Mo-NiMo/NF, Mo/NF and NF at 20 mA cm^{-2} (defined as η20) were described as 102 mV, 150 mV and 271 mV, respectively. And the value order of the results was in accordance with that of η10. Therefore, it was suggested that Mo-NiMo/NF showed best electrochemical performance, which might be attributed to the formation of NiMo alloy and heterojunction (between NiMo and Mo) after the annealing.

It was well known that the Tafel slope was directly related with the HER reaction kinetics of electrocatalyst, the smaller Tafel slope meant faster kinetics and superior catalytic performance [23]. Fig. 6b exhibited the HER Tafel slopes of the Mo-NiMo/NF, Mo/NF and pristine NF from the polarization curves. The linear regions of Tafel plots were fitted by the Tafel equation: $\eta = a + b\log(j)$ (in which η was the overpotential, a was the Tafel constant, b was the Tafel slope and j was the current density). The Mo-NiMo/NF showed a Tafel slope of 104 $mVdec^{-1}$, which was smaller than those of many previously reported electrocatalysts such as Ni-Mo-Cu alloy [60] and NiMo coating [33], indicating a higher HER rate and faster kinetics. Furthermore, the Tafel slope fell within the scale of 40–120 $mVdec^{-1}$, suggesting that the HER process on Mo /NF and Mo-NiMo/NF followed the Volmer–Heyrovsky regulation [61].

In order to get further insight into the kinetics of charge transfer, the EIS studies of the prepared electrodes in the frequency scope of 10^5–0.01 Hz at an overpotential of η = 200 mV were carried out. Fig. 6c showed the Nyquist plots and the equivalent circuit modeling for the electrochemical impedance data as inset. The results clearly indicated the changes in the arc diameter. The Mo-NiMo/NF electrode disclosed the smallest charge transfer resistances (R_{ct}) of 0.28 Ω, compared with those of NF (1.21 Ω) and Mo/NF (0.98 Ω), indicating a markedly fast Faradaic process and favorable HER kinetics [7]. It might mainly be due to the change of element distribution in the coating and the change of interface structure between coating and substrate after annealing (Fig. 4). The close combination between substrate and coating resulted in a fast electronic transmission and a small R_{ct} after the annealing.

It was also known that the electrochemical stability was another important parameter of evaluating the feasibility for the practical application. To better understand the stability of the Mo-NiMo/NF electrode, the CA experiment at an overpotential (71 mV) for 24 h was performed (Fig. 6d). It was observed that the current density was only 1.0% reduction, showing an excellent durability.

Table 1
HER performance data for as-synthesized samples.

Catalysts	η10[a] (mV)	η20[b] (mV)	Tafel slope (mV/decade)
NF	212	271	195
Mo/NF	91	150	115
Mo-NiMo/NF	71	102	104

[a] η10: The overpotential at a current density of 10 mA cm^{-2}.
[b] η20: The overpotential at a current density of 20 mA cm^{-2}.

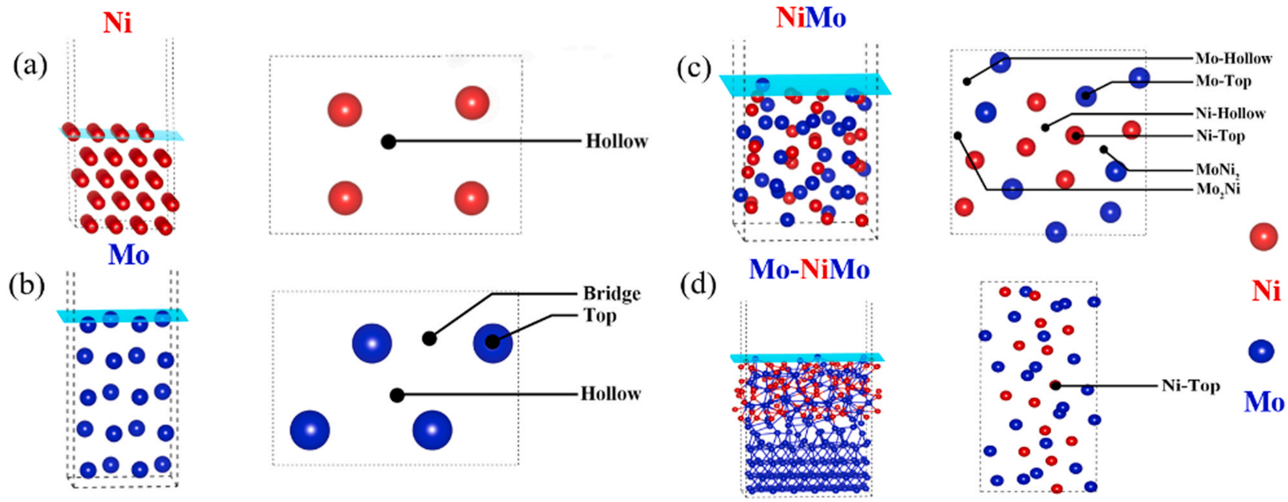

Fig. 7. The optimized structures of H* adsorption sites for Ni (a), Mo (b), NiMo (c) and Mo-NiMo heterostructure (d).

According to above analysis, the reactions on Mo/NF and Mo-NiMo/NF followed the Volmer–Heyrovsky mechanism as follows:[7].

Volmer reaction: $e^- + H_2O \rightarrow H^* + OH^-$ (Hydrogen adsorption) (S5)

Heyrovsky reaction: $2H^* + e^- \rightarrow H_2$ (Electrochemical desorption) (S6)

Therefore, the adsorbed hydrogen atom played a key role in the thermodynamics and kinetics of the HER, and the strength of proton adsorption bonding to the metal surface was important for the reaction rate during the HER. Moreover, based on the Sabatier principle [62], the catalyst possessed a moderate ΔG_{H^*} could show excellent hydrogen evolution performance. The closer ΔG_{H^*} to zero, the better advantage to both the H*adsorption and H_2 desorption process for the hydrogen evolution. Therefore, the DFT computation had been applied to calculate the ΔE_{H^*} and ΔG_{H^*} to study the mechanisms of superior electrocatalytic performance.

The adopted crystal structures of Ni and Mo were based on the results of XRD. As for NiMo, it was assumed that the NiMo system was dominated by the form of $Ni_{24}(Ni_4Mo_{16})Mo_{12}$ [63,64]. Based on previous report [61], (111), (110) and (100) lattice planes were adopted as the exposed surface for Ni, Mo and NiMo. The thickness of Ni and Mo slab model was 5 layers, with the bottom 2 layers of atoms fixed to simulate bulk component, as well as the thickness of NiMo slab was the same as the lattice constant. (Fig. 7a-c). Moreover, a vacuum layer sized in 15 Å was added along z axis in the slab models. The hydrogen atom was then placed at different adsorption sites of these slabs. All the calculated ΔE_{H^*} and ΔG_{H^*} of catalyst samples were shown in Table 2**.** The calculated results indicated that the optimal adsorption sites for Ni, Mo and NiMo were hollow, bridge and Ni2Mo sites, respectively. Consequently, the adsorption site for Mo-NiMo heterostructure was also chosen as Ni2Mo site (Fig. 7d).

Table 2
The calculated ΔE_{H^*} and ΔG_{H^*} of Ni, Mo, NiMo and Mo-NiMo heterostructure.

Catalysts	Adsorption sites	ΔE_{H^*} (eV)	ΔG_{H^*} (eV)
Ni	Hollow	-0.3.9	-0.384
Mo	Top	-3.097	-2.857
	Bridge	-1.832	-1.592
	Hollow	-1.909	-1.669
NiMo	Mo-top	-0.328	-0.088
	Mo2Ni	-0.160	0.080
	Mo3	-0.025	0.215
	Ni-top	-0.343	-0.103
	Ni2Mo	-0.267	-0.027
	Ni3	-0.123	0.117
Heterostructure	Ni-Top	-1.786	-1.546

As shown in Table 2, the Mo had the most negative ΔE_{H^*}, (−3.097 eV) compared with NF (−0.39 eV), which was conducive to the Volmer reaction. That was to say that the adsorption of hydrogen ions was promoted in the reaction due to the Mo addition on the surface of NF. Similarly, the heterojunction between Mo and NiMo provided the negative ΔE_{H^*} of − 1.786 eV, which also could facilitate Volmer step to further accelerate HER performance. More importantly, in view of the Sabatier principle, the results in Fig. 8**a and b** presented that the values on ΔG_{H^*} of NiMo were much closer to zero than that of Ni (−0.384 eV), suggesting that the introduction of Mo atoms in NF highly enhanced both the H*adsorption and H_2 desorption process for the hydrogen evolution. The DFT simulations showed no difference with the experimental results that the Mo-NiMo/NF and Mo/NF owned the best and better HER activities respectively among the prepared electrodes. Moreover, the phenomenon was also consistent with the Engel–Brewer valence bond theory [65]. The transition metals with empty or less-filled d orbitals (e.g., Mo) were alloyed with those with more-filled d orbitals (e.g., Ni), a synergistic effect in the hydrogen evolving activity of these materials was appeared [35]. Fig. 8c showed an illustration of the enhanced HER by the catalyst samples.

In view of the above results, the outstanding HER electrocatalytic performance of the Mo-NiMo/NF could be summed up. On the one hand, based on the advantages of the substrate NF, the prepared catalyst owned the 3D microporous structure, which could both maximize the contact area with the alkaline solution and increased numbers of exposed active sites. On the other hand, in terms of composition design, the presence of Mo and the heterojunction between Mo and NiMo could promote the Volmer reaction, and NiMo alloy enhanced both Volmer reaction and Heyrovsky reaction, which might lead to a synergistic effect to further contribute to the electrocatalytic performance for HER. With such composition of the alloys, the H_2 production was accelerated, leading to faster HER kinetics and better catalytic activity. In a word, the easy-fabrication,

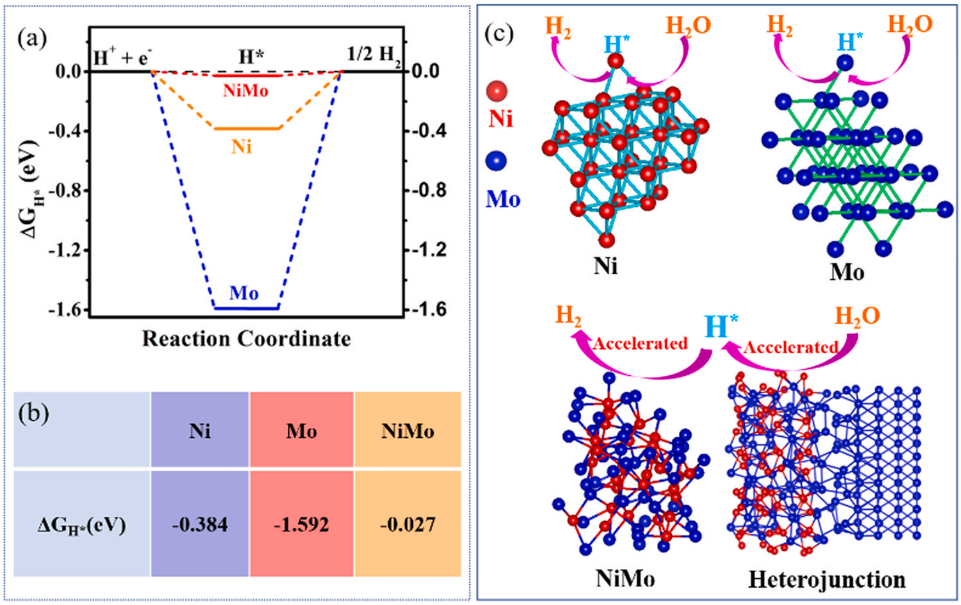

Fig. 8. DFT simulations of Gibbs free energy and the mechanisms of the electrocatalytic HER. (a) and (b) Gibbs free energy diagram of HER at the equilibrium potential for catalyst samples. (c) Elucidation of the enhanced HER mechanism by the catalyst samples. H* denotes that intermediate adsorbed hydrogen.

high electrocatalytic activity, and good stability endowed Mo-NiMo/NF with potential application in alkaline hydrogen evolution.

4. Conclusions

In this study, the Mo-NiMo/NF cathode was obtained by a facile and effective technique HiPIMS along with vacuum annealing. This novel method offered a very simple and large-scale manufacturing way to fabricate antioxidation low-cost HER cathodes. The fabricated Mo-NiMo/NF showed a high catalytic performance and an outstanding long-term stability for HER in alkaline media. The DFT confirmed that the HER catalytic activity was due to the presences of Mo and NiMo in the electrode. The Mo and the heterojunction between Mo and NiMo owned the more negative ΔE_{H^*} values, which could optimize adsorption of H* to promote the Volmer reaction in HER. And the NiMo alloy promoted the activity because of the near-zero ΔG_{H^*}. A synergistic effect of optimized adsorption-desorption was supposed to contribute to the electrocatalytic performance of HER. This study here could prompt further potential and practical viability of Ni-based alloys on the intrinsic active sites and the synergistic effects of the bimetallic catalysts for HER.

CRediT authorship contribution statement

Guanshui Ma: Conceptualization, Validation, Formal analysis, Investigation, Data curation, Writing – original draft, Visualization. **Yapeng Zheng:** Formal analysis, Writing – review & editing. **Jiayue Zhang:** Software, Investigation. **Jiangshan Yan:** Investigation, Data curation, Writing – review & editing, Project administration. **Peng Guo:** Investigation, Writing – review & editing. **Wei Yang:** Writing – review & editing. **Rende Chen:** Investigation, Methodology. **Jianghuai Yuan:** Investigation. **Li Cui:** Investigation. **Aiying Wang:** Resources, Writing – review & editing, Visualization, Project administration, Funding acquisition.

Data availability

The authors do not have permission to share data.

Declaration of Competing Interest

The authors declare that they have no known competing financial interests or personal relationships that could have appeared to influence the work reported in this paper.

Acknowledgements

The work was supported by the National Natural Science Foundation of China Science Foundation of China (No. 52101109), the K.C. Wong Education Foundation (No. GJTD-2019-13), the Zhejiang Lingyan Research and Development Program (No. 2022C01113), the Zhejiang Provincial Natural Science Foundation of China (No. LQ20E020004). G. S. Ma would like to thank Abdullah Flehan for his contribution to the english polishing.

Appendix A. supporting information

Supplementary data associated with this article can be found in the online version at doi:10.1016/j.jallcom.2022.167855.

References

[1] Q. Gao, W. Zhang, Z. Shi, L. Yang, Y. Tang, Structural design and electronic modulation of transition-metal-carbide electrocatalysts toward efficient hydrogen evolution, Adv. Mater. 31 (2019) e1802880.
[2] J. Park, T.H. Ko, S. Balasubramaniam, M.K. Se, M.S. Khil, H.Y. Kim, B.S. Kim, Enhancing the performance and stability of $NiCo_2O_4$ nanoneedle coated on Ni foam electrodes with Ni seed layer for supercapacitor applications, Ceram. Int. 45 (2019) 13099–13111.
[3] L.X. Zan, H.L. Zhang, X. Bo, Y.Y. Zhao, H.Q. Tian, H. Chen, Q.B. Wei, H.Q. Tang, F. Fu, Investigation of the synergistic effect on cobalt oxide modified silver surface for electrocatalytic hydrogen evolution reaction, J. Alloy. Compd. 869 (2021) e159324.
[4] Y. Wu, Y. Yang, Y. Li, C. Zhang, Y. Wang, H. Tian, Highly efficient hybrid electrocatalyst $Fe_{4.5}Ni_{4.5}S_8/Fe_7S_8$ extracted from nickel ore for hydrogen evolution reaction, Ceram. Int. 47 (2021) 12002–12009.
[5] J.L. Zheng, K.L. Wu, C. Lyu, X. Pan, X.F. Zhang, Y.C. Zhu, A.D. Wang, W.M. Lau, N. Wang, Electrocatalyst of two-dimensional CoP nanosheets embedded by carbon nanoparticles for hydrogen generation and urea oxidation in alkaline solution, Appl. Surf. Sci. 506 (2020) e144997.
[6] H. Park, I.J. Park, M.G. Lee, K.C. Kwon, S.P. Hong, D.H. Kim, S.A. Lee, T.H. Lee, C. Kim, C.W. Moon, D.Y. Son, G.H. Jung, H.S. Yang, J.R. Lee, J. Lee, N.G. Park, S.Y. Kim, J.Y. Kim, H.W. Jang, Water splitting exceeding 17% solar-to-hydrogen conversion efficiency using solution-processed Ni-based electrocatalysts and

perovskite/Si Tandem solar cell, ACS Appl. Mater. Interfaces 11 (2019) 33835–33843.

[7] J. Yu, A.R. Li, L.D. Li, X. Li, X.T. Wang, L. Guo, Morphological and structural engineering in amorphous Cu_2MoS_4 nanocages for remarkable electrocatalytic hydrogen evolution, Sci. China Mater. 62 (2019) 1275–1284.

[8] J.W. Chen, Y.C. Ling, D.Q. Qu, L.N. Huang, J.J. Li, P.J. Tang, A.P. He, X. Jin, Y. Zhou, M.X. Xu, J. Du, Z.D. Han, Q.Y. Xu, Enhanced electrocatalysis of NiMnIn Heusler alloy films for hydrogen evolution reaction by magnetic field, J. Alloy. Compd. 877 (2021) e160271.

[9] J. Zhu, L. Hu, P. Zhao, L.Y.S. Lee, K.Y. Wong, Recent advances in electrocatalytic hydrogen evolution using nanoparticles, Chem. Rev. 120 (2020) 851–918.

[10] G.S. Ma, Y.W. He, M. Wang, F.C. Zhu, B. Tang, X.G. Wang, An efficient route for catalytic activity promotion via hybrid electro-depositional modification on commercial nickel foam for hydrogen evolution reaction in alkaline water electrolysis, Appl. Surf. Sci. 313 (2014) 512–523.

[11] S. Sarika, S. Abhilash, V.S. Sumi, S. Rijith, Graphene oxide supported transition metal mixed oxide nanourchins onto bimetallic phosphide coatings as high performance hydrogen evolution electrodes in alkaline media, J. Alloy. Compd. 875 (2021) e160033.

[12] H.L.S. Santos, P.G. Corradini, M. Medina, J.A. Dias, L.H. Mascaro, NiMo-NiCu inexpensive composite with high activity for hydrogen evolution reaction, ACS Appl. Mater. Interfaces 12 (2020) 17492–17501.

[13] Z.Z. Ma, H.J. Meng, M. Wang, B. Tang, J.P. Li, X.G. Wang, Porous Ni−Mo−S nanowire network film electrode as a high-efficiency bifunctional electrocatalyst for overall water splitting, Chem. Electro Chem. 5 (2018) 335–342.

[14] Z.Z. Ma, R. Li, M. Wang, H. Meng, F. Zhang, X.Q. Bao, B. Tang, X.G. Wang, Self-supported porous Ni-Fe-P composite as an efficient electrocatalyst for hydrogen evolution reaction in both acidic and alkaline medium, Electrochim. Acta 219 (2016) 194–203.

[15] J.L. Zheng, W. Zhou, T. Liu, S. Liu, C. Wang, L. Guo, Homologous NiO//Ni_2P nanoarrays grown on nickel foams: a well matched electrode pair with high stability in overall water splitting, Nanoscale 9 (2017) 4409–4418.

[16] X. Yi, X. He, F. Yin, G. Li, Z. Li, Surface strain engineered Ni-NiO for boosting hydrogen evolution reaction in alkaline media, Electrochim. Acta 391 (2021) e138985.

[17] X.Y. Yu, Y. Feng, Y. Jeon, B. Guan, X.W. Lou, U. Paik, Formation of Ni-Co-MoS_2 nanoboxes with enhanced electrocatalytic activity for hydrogen evolution, Adv. Mater. 28 (2016) 9006–9011.

[18] Q. Zhou, S. Liu, Y. Zhang, Z. Zhu, W. Su, M. Sheng, Fabrication of porous Cu supported Ni-P/CeO_2 composite coatings for enhanced hydrogen evolution reaction in alkaline solution, Ceram. Int. 46 (2020) 20871–20877.

[19] T. Liu, A. Li, C. Wang, W. Zhou, S. Liu, L. Guo, Interfacial electron transfer of Ni_2P-NiP_2 polymorphs inducing enhanced electrochemical properties, Adv. Mater. 30 (2018) e1803590.

[20] Z. Jin, T. Wei, F. Li, Q. Zhang, L. Xu, Fabrication of a novel Ni_3N/Ni_4N heterojunction as a non-noble metal co-catalyst to boost the H_2 evolution efficiency of Zn0.5Cd0.5S, New J. Chem. 44 (2020) 3471–3477.

[21] D. Gao, J. Zhang, T. Wang, W. Xiao, K. Tao, D. Xue, J. Ding, Metallic Ni_3N nanosheets with exposed active surface sites for efficient hydrogen evolution, J. Mater. Chem. A 4 (2016) 17363–17369.

[22] Y. Ma, Z. He, Z. Wu, B. Zhang, Y. Zhang, S. Ding, C. Xiao, Galvanic-replacement mediated synthesis of copper–nickel nitrides as electrocatalyst for hydrogen evolution reaction, J. Mater. Chem. A 5 (2017) 24850–24858.

[23] B. Liu, B. He, H.Q. Peng, Y. Zhao, J. Cheng, J. Xia, J. Shen, T.W. Ng, X. Meng, C.S. Lee, W. Zhang, Unconventional nickel nitride enriched with nitrogen vacancies as a High-Efficiency electrocatalyst for hydrogen evolution, Adv. Sci. 5 (2018) e1800406.

[24] W.N. Liu, T.Y. Xia, Y.M. Ye, H. Wang, Z. Fang, Z.T. Du, X.M. Hou, Self-supported Ni_3N nanoarray as an efficient nonnoble-metal catalyst for alkaline hydrogen evolution reaction, Int. J. Hydrog. Energy 46 (2021) 27037–27043.

[25] M. Wang, H. Yang, J. Shi, Y. Chen, Y. Zhou, L. Wang, S. Di, X. Zhao, J. Zhong, T. Cheng, W. Zhou, Y. Li, Alloying nickel with molybdenum significantly accelerates alkaline hydrogen electrocatalysis, Angew. Chem. Int. Ed. 60 (2021) 5771–5777.

[26] Y.Q. Wang, L. Zhao, X.L. Sui, D.M. Gu, Z.B. Wang, Hierarchical $CoP_3/NiMoO_4$ heterostructures on Ni foam as an efficient bifunctional electrocatalyst for overall water splitting, Ceram. Int. 45 (2019) 17128–17136.

[27] L. Ma, L.R.L. Ting, V. Molinari, C. Giordano, B.S. Yeo, Efficient hydrogen evolution reaction catalyzed by molybdenum carbide and molybdenum nitride nanocatalysts synthesized via the urea glass route, J. Mater. Chem. A 3 (2015) 8361–8368.

[28] J.G. Zhang, S.M. Zhang, S. Li, H. Dai, Q. Hu, B. Zhang, L.M. Wang, Electrocatalytic properties of nickel foam-based Ni-Mo, Ni+Mo and Ni+Mo/Ni-Mo electrodes for hydrogen evolution reaction, Mater. Sci. Forum 921 (2018) 134–140.

[29] A. Toghraei, T. Shahrabi, G. Barati Darband, Electrodeposition of self-supported Ni-Mo-P film on Ni foam as an affordable and high-performance electrocatalyst toward hydrogen evolution reaction, Electrochim. Acta 335 (2020) e135643.

[30] C. Li, J. Wang, Y. Wang, J. Li, Z. Yao, Z. Jiang, Enhancing hydrogen evolution reaction by synergistically coupling NiMo alloy with $Ni(OH)_2$ nanosheet on carbon cloth, Chem. Sel. 5 (2020) 6774–6779.

[31] Q. Yao, Z.H. Lu, W. Huang, X. Chen, J. Zhu, High Pt-like activity of the Ni–Mo/graphene catalyst for hydrogen evolution from hydrolysis of ammonia borane, J. Mater. Chem. A 4 (2016) 8579–8583.

[32] S. Shetty, A.C. Hegde, Magnetically induced electrodeposition of Ni-Mo alloy for hydrogen evolution reaction, Electrocatalysis 8 (2017) 179–188.

[33] M. Wang, Z. Wang, X. Yu, Z. Guo, Facile one-step electrodeposition preparation of porous NiMo film as electrocatalyst for hydrogen evolution reaction, Int. J. Hydrog. Energy 40 (2015) 2173–2181.

[34] W. Du, Y. Shi, W. Zhou, Y. Yu, B. Zhang, Unveiling the in situ dissolution and polymerization of Mo in Ni_4Mo alloy for promoting the hydrogen evolution reaction, Angew. Chem. Int. Ed. 60 (2021) 7051–7055.

[35] M. Manazoğlu, G. Hapçı, G. Orhan, Effect of electrolysis parameters of Ni–Mo alloy on the electrocatalytic activity for hydrogen evaluation and their stability in alkali medium, J. Appl. Electrochem. 46 (2015) 191–204.

[36] D.O.P. Kedzierzawski, M. Janik-Czachor, Hydrogen evolution on hot and cold consolidated Ni–Mo alloys, Mater. Sci. Eng. 300 (2001) 105–112.

[37] L. Rodríguez-Valdez, Electrochemical performance of hydrogen evolution reaction of Ni–Mo electrodes obtained by mechanical alloying, Int. J. Hydrog. Energy 29 (2004) 1141–1145.

[38] S. Sun, E.J. Podlaha, Electrodeposition of Mo-rich, MoNi alloys from an aqueous electrolyte, J. Electrochem. Soc. 159 (2011) 97–102.

[39] A. Lasia, D. Miousse, Hydrogen evolution reaction on Ni-Al-Mo and Ni-Al electrodes prepared by low pressure plasma spraying, J. Appl. Electrochem. 25 (1995) 592–602.

[40] D. Oleszak, V.K. Portnoy, H. Matyja, Formation of metastable phases in Ni-43·5at Mo powder mixtures during mechanical alloying and after heat treatment, Philos. Mag. B 76 (2006) 639–649.

[41] S.J. Gutić, A.Z. Jovanović, A.S. Dobrota, D. Metarapi, L.D. Rafailović, I.A. Pašti, S.V. Mentus, Simple routes for the improvement of hydrogen evolution activity of Ni-Mo catalysts: from sol-gel derived powder catalysts to graphene supported co-electrodeposits, Int. J. Hydrog. Energy 43 (2018) 16846–16858.

[42] S. Mentus, B. Tomić-Tucaković, D. Majstorović, R. Dimitrijević, Gel-combustion synthesis of NiO–MoO_3 mixtures and their reduction to Ni–Mo alloys, Mater. Chem. Phys. 112 (2008) 254–261.

[43] C.E. Yaldiz, R. Veinthal, A. Gregor, K. Georgiadis, Mechanical properties of thin hard coatings on TiC-NiMo substrates, J. Eng. Technol. 15 (2009) 329–339.

[44] N.M. Lin, X.B. Huang, X. Zhang, A. Fan, L. Qin, B. Tang, In vitro assessments on bacterial adhesion and corrosion performance of TiN coating on Ti6Al4V titanium alloy synthesized by multi-arc ion plating, Appl. Surf. Sci. 258 (2012) 7047–7051.

[45] N.M. Lin, X. Huang, J.J. Zou, X. Zhang, L. Qin, A. Fan, B. Tang, Effects of plasma nitriding and multiple arc ion plating TiN coating on bacterial adhesion of commercial pure titanium via in vitro investigations, Surf. Coat. Technol. 209 (2012) 212–215.

[46] X. Zuo, D. Zhang, R. Chen, P.L. Ke, M. Odén, A. Wang, Spectroscopic investigation on the near-substrate plasma characteristics of chromium HiPIMS in low density discharge mode, Plasma Sources Sci. Technol. 29 (2020).

[47] V. Stranak, J. Kratochvil, J. Olejnicek, P. Ksirova, P. Sezemsky, M. Cada, Z. Hubicka, Enhanced oxidation of TiO_2 films prepared by high power impulse magnetron sputtering running in metallic mode, J. Appl. Phys. 121 (2017) e171914.

[48] G. Kresse, J. Hafner, Ab initio molecular dynamics for open-shell transition metals, Phys. Rev. B 48 (1993) 13115–13118.

[49] G.K.J. Furthmu¨ller, Efficient iterative schemes for Ab initio total-energy calculations using a plane-wave basis set, Phys. Rev. B 54 (1996) 169–186.

[50] P.E. Blochl, Projector augmented-wave method, Phys. Rev. B 50 (1994) 17953–17979.

[51] J.P. Perdew, K. Burke, M. Ernzerhof, Generalized gradient approximation made simple, Phys. Rev. Lett. 77 (1996) 3865–3868.

[52] S. Grimme, S. Ehrlich, L. Goerigk, Effect of the damping function in dispersion corrected density functional theory, J. Comput. Chem. 32 (2011) 1456–1465.

[53] S. Grimme, J. Antony, S. Ehrlich, H. Krieg, A consistent and accurate ab initio parametrization of density functional dispersion correction (DFT-D) for the 94 elements H-Pu, J. Chem. Phys. 132 (2010) e154104.

[54] A. Rohrbach, J. Hafner, G. Kresse, Molecular adsorption on the surface of strongly correlated transition-metal oxides: a case study for CO/NiO (100), Phys. Rev. B 69 (2004) e075413.

[55] R. Coquet, D.J. Willock, The (010) surface of alpha-MoO3, a DFT+U study, Phys. Chem. Chem. Phys. 7 (2005) 3819–3828.

[56] K. Ojha, M. Sharma, H. Kolev, A.K. Ganguli, Reduced graphene oxide and MoP composite as highly efficient and durable electrocatalyst for hydrogen evolution in both acidic and alkaline media, Catal. Sci. Technol. 7 (2017) 668–676.

[57] L. Yang, L. Zeng, H. Liu, Y. Deng, Z. Zhou, J. Yu, H. Liu, W. Zhou, Hierarchical microsphere of MoNi porous nanosheets as electrocatalyst and cocatalyst for hydrogen evolution reaction, Appl. Catal. B 249 (2019) 98–105.

[58] Z. Chang, L. Zhu, J. Zhao, P. Chen, D. Chen, H. Gao, NiMo/Cu-nanosheets/Ni-foam composite as a high performance electrocatalyst for hydrogen evolution over a wide pH range, Int. J. Hydrog. Energy 46 (2021) 3493–3503.

[59] Q. Han, S. Cui, N. Pu, J. Chen, K. Liu, X. Wei, A study on pulse plating amorphous Ni–Mo alloy coating used as HER cathode in alkaline medium, Int. J. Hydrog. Energy 35 (2010) 5194–5201.

[60] M. Xia, T. Lei, N. Lv, N. Li, Synthesis and electrocatalytic hydrogen evolution performance of Ni–Mo–Cu alloy coating electrode, Int. J. Hydrog. Energy 39 (2014) 4794–4802.

[61] G.S. Ma, P. Guo, S.Y. Wang, Y. Liu, Y. Xin, H. Li, R.D. Chen, A.Y. Wang, One-step plasma nitriding synthesis of Ni_xN/NF (x=3, 4) for efficient hydrogen evolution, Appl. Surf. Sci. 561 (2021) e149972.

[62] Y.Y. Ma, C.X. Wu, X.J. Feng, H.Q. Tan, L.K. Yan, Y. Liu, Z.H. Kang, E.B. Wang, Y.G. Li, Highly efficient hydrogen evolution from seawater by a low-cost and stable CoMoP@C electrocatalyst superior to Pt/C, Energy Environ. Sci. 10 (2017) 788–798.

[63] Y. Ito, T. Ohto, D. Hojo, M. Wakisaka, Y. Nagata, L. Chen, K. Hu, M. Izumi, J. Fujita, T. Adschiri, Cooperation between holey graphene and NiMo alloy for hydrogen evolution in an acidic electrolyte, ACS Catal. 8 (2018) 3579–3586.

[64] Y. Wang, C. Woodward, S.H. Zhou, Z.K. Liu, L.Q. Chen, Structural stability of Ni–Mo compounds from first-principles calculations, Scr. Mater. 52 (2005) 17–20.

[65] C.C. Hu, C.Y. Weng, Hydrogen evolving activity on nickel-molybdenum deposits using experimental strategies, J. Appl. Electrochem. 30 (2000) 499–506.